Technical Note

Modeling Bridges in HEC-RAS 2D: Comparison with Flume Experiments

Gabriele Farina[1]; Marco Pilotti, Ph.D.[2]; Riccardo Bonomelli, Ph.D.[3]; Sergio Martínez-Aranda, Ph.D.[4]; and Pilar García-Navarro, Ph.D.[5]

Abstract: A set of experimental measurements with a physical model in a flume, measuring the head loss generated by different bridge geometries in steady and unsteady conditions, is used to test the performance of HEC-RAS 2D in modeling bridge hydraulics, a fundamental component of any flood study. After upscaling the experimental results according to Froude similarity, the numerical tests have explored the effects of the choice of the options offered by the HEC-RAS 2D software with the default value of the parameters and the obtainable improvement when the geometry of the bridges suggested a customized value of parameters. The numerical results show a very good match with the measured water elevation upstream of the bridges for almost all tested cases. The mean absolute percentage error obtained pooling all the steady test cases is less than 5%. **DOI: 10.1061/JHEND8.HYENG-14354.** © *2025 American Society of Civil Engineers.*

Practical Applications: Computational models have become essential tools in flood modeling, with a growing body of scientific research over the past few decades. Among the many available models, HEC-RAS stands out as a widely accepted software for both one-dimensional (cross-sectional averaged flow) and two-dimensional (2D) (depth-averaged flow) simulations. This is due to its comprehensive range of features, which aid in modeling real-world scenarios. Like any computational model, HEC-RAS requires thorough validation and verification against measured data, whenever such data are available. The present study focuses on evaluating the performance of HEC-RAS 2D for simulating steady and unsteady open channel flow in the presence of bridges, comparing its results with respect to a wide set of laboratory data. Bridges play a crucial role in the flooding process, and accurately modeling their hydraulic behavior is essential for reliably reproducing flood dynamics. The obtained numerical results show an excellent match with the measurements in nearly all tested cases, also offering valuable insights for selecting model parameters.

Author keywords: Bridge modeling; HEC-RAS 2D; Flood studies; Physical models.

Introduction

In recent decades, significant attention has been devoted to developing reliable two-dimensional (2D) shallow water equation (SWE) solvers, driven by the need for accurate flood hazard mapping due to increasing anthropic pressure and climate extremes (Mudashiru et al. 2021). This progress has been supported by advancements in data collection methods, such as terrestrial and remote surveying techniques, as well as improvements in computational power, often utilizing high-performance computing (e.g., Costabile et al. 2023; Caviedes-Voullième et al. 2023). It is well known that one of the most important stumbling blocks in a 2D simulation of a flood propagation is a correct representation of bridges within the computational domain because the backwater effect caused by the presence of a bridge structure is essential for the definition of flooded areas. Whereas the reproduction of local details of flow around the bridge requires a three-dimensional (3D) modeling approach (e.g., Chu et al. 2016; Lai et al. 2022), the overall energy losses in the modeling areas can be well reproduced using the approximation at the basis of the 2D SWE.

In literature, four different types of bridge representation in 2D numerical models were explored (Mckenna et al. 2023; Cea et al. 2022 and references therein): (1) with reference to low-flow conditions only, by applying a detailed mesh discretization around the piers and abutments of the bridge: in this case the pressurized flow regime is not considered and the typical size of the grid refinement around the bridge directly affects the time step, increasing the computational time; (2) by introducing a head loss as an additional source term in the governing equations (e.g., Ratia et al. 2014); (3) as an internal boundary condition (Dazzi et al. 2020) where appropriate discharge formulas that describe the hydraulics of the bridge are imposed at cells boundary along a polyline representing the structure; and (4) by the Preissmann slot, which can be extended to 2D SWE to solve the pressurized flow (Maranzoni and Mignosa 2018; Cea et al. 2022). Neither the first nor the fourth mode can account for the overflow condition.

In this direction, the widely used SWE solver HEC-RAS 2D was recently released (from Version 6.0) with the option to lay

[1]Ph.D. Candidate, Dept. of Civil, Environmental, Architectural Engineering and Mathematics, Università degli Studi di Brescia, Brescia 25123, Italy (corresponding author). ORCID: https://orcid.org/0000-0002-1899-6366. Email: gabriele.farina@unibs.it

[2]Full Professor, Dept. of Civil, Environmental, Architectural Engineering and Mathematics, Università degli Studi di Brescia, Brescia 25123, Italy. ORCID: https://orcid.org/0000-0001-9349-0851. Email: marco.pilotti@unibs.it

[3]Research Fellow, Dept. of Civil, Environmental, Architectural Engineering and Mathematics, Università degli Studi di Brescia, Brescia 25123, Italy. ORCID: https://orcid.org/0000-0003-0412-5778. Email: riccardo.bonomelli@unibs.it

[4]Assistant Professor, TFD Group, I3A, Universidad de Zaragoza, Zaragoza 50018, Spain. ORCID: https://orcid.org/0000-0003-4673-9073. Email: sermar@unizar.es

[5]Full Professor, TFD Group, I3A, Universidad de Zaragoza, Zaragoza 50018, Spain. ORCID: https://orcid.org/0000-0001-8674-1042. Email: pigar@unizar.es

Note. This manuscript was submitted on September 12, 2024; approved on June 3, 2025; published online on September 17, 2025. Discussion period open until February 17, 2026; separate discussions must be submitted for individual papers. This technical note is part of the ***Journal of Hydraulic Engineering***, © ASCE, ISSN 0733-9429.

out bridges inside a 2D flow area. The novel approach can be used for all flow regimes (low flow, pressure flow, overtopping in the possible combinations; Brunner 2020). Although this approach relies on the curves for modeling bridges that are computed as in the widely tested one-dimensional (1D) version of HEC-RAS, the performance of these procedures could be different when they are introduced in a 2D unstructured code, where there are complex problems of coupling with the surrounding cells. For instance, the 1D model relies on two additional user-defined cross sections placed upstream and downstream the bridge where the flow is fully expanded. This step is not present in the 2D model where it is dealt with by the surrounding grid. Moreover, the bridge curves used for unsteady flow are built in steady flow conditions.

Finally, the choice of a modeling method for bridge hydraulics and of the parameters involved in the computation is required, for which a default value is suggested by the program along with a possible range of variation. Although there is a considerable body of literature that can assist in the selection of the method and in the calibration (e.g., Bradley 1978), it is sometimes difficult, even for the experienced user, to appreciate in advance the implication of the possible options (Seckin et al. 2007).

HEC-RAS 2D is released along with a set of validation test cases (Brunner et al. 2020), and it is continually tested by comparison with the results of physical models and other SWE solvers to understand the performance of the model in challenging problems (e.g., Pilotti et al. 2020; Milanesi and Pilotti 2021; Costabile et al. 2021; Darji et al. 2024), contributing to improving its predictive effectiveness. However, until now no systematic test of the novel approach for bridge hydraulics in HEC-RAS 2D has been conducted in the literature. In this paper a contribution to fill this gap is provided, using the experimental results of a physical model in a flume for 15 different bridge geometries in steady flow experiments and 8 bridge geometries in unsteady flow (Ratia et al. 2014). These two large datasets allow us to test the performance of bridge modeling in HEC-RAS 2D for both steady and unsteady conditions and provide insights on the practical consequences of the different options that can be selected for this task within the program.

Experimental Test and Physical Model Upscaling According to Froude Similarity

The experimental results by Ratia et al. (2014) have been used in several numerical studies (e.g., Maranzoni and Mignosa 2018; Cea and López-Núñez, 2021; Dazzi et al. 2020; Petaccia and Persi 2024). The experiments were performed in a laboratory flume where the water level upstream and downstream of a bridge was measured for 15 different geometries in steady flow experiments and for 8 bridge geometries in unsteady flow (Ratia et al. 2014). All the details related to the experimental setup and the geometry of the bridges are provided in the Supplemental Materials (Figs. S1–S4). The typical water depths upstream of the bridges in the rectangular cross section of the flume used by Ratia et al. (2014) range between 0.014 and 0.124 m. On the other hand, HEC-RAS 2D has been mainly applied to field-scale cases, and based on our experience, it is uncertain whether it can process input data related to small-scale experiments, with discharges less than 1 L s^{-1}. To overcome this stumbling block, the following procedure has been adopted. Considering that 90% of the 207 experiments accomplished by Ratia et al. (2014) are in the range $R > 10^4$, with $R \leq 5{,}000$ for 3% of the cases only, it is adequate (e.g., Chanson 2004) to rescale the experimental results respecting Froude similarity only:

$$\frac{v_m}{\sqrt{gL_m}} = \frac{v_p}{\sqrt{gL_p}} \tag{1}$$

where m = HEC-RAS 2D model; p = physical model; L = characteristic length; and v = velocity. By introducing the length scale $\lambda_l = L_m/L_p$ adopted for the model geometry, from Eq. (1) one gets the velocity ratio $\lambda_v = v_m/v_p = \lambda_l^{1/2}$ and the time ratio $\lambda_t = t_m/t_p = \lambda_l^{1/2}$, and it is eventually possible to define the two scale ratios for the volumetric discharge and the Manning roughness coefficient: $\lambda_Q = Q_m/Q_p = \lambda_l^{5/2}$ and $\lambda_n = n_m/n_p = \lambda_l^{1/6}$. In conclusion, the geometry of the HEC-RAS 2D model was built assuming a length scale $\lambda_l = 20$ for the undistorted representation of the laboratory flume. For a limited set of steady-state cases, the choice $\lambda_l = 50$ has been explored, with no significative difference in the obtained results. The corresponding values of the ratios λ_t, λ_Q, and λ_n were used to upscale the geometry and the boundary conditions to be used in all the HEC-RAS 2D simulations. For the final comparison with the experimental results, the HEC-RAS 2D results were downscaled to the physical model scale.

Numerical Model: HEC-RAS 2D

HEC-RAS 2D solves the 2D SWE with a combination of finite-difference and finite-volume methods on a structured or unstructured mesh operating with different sets of equations (Brunner 2020). The Eulerian SWE-EM solver was used for all the simulations because it is more conservative, especially in lab simulations where strict conservation of momentum is important (Brunner 2020). In the following, HEC-RAS 6.3.1 was used, and the analysis for each bridge was conducted using the energy method approach for low-flow conditions, due to its greater generality with respect to Yarnell and momentum methods. On the other hand, both the energy method and the pressure-and-weir method (Brunner 2020) were tested for high-flow conditions. All the numerical simulations were accomplished using the default value of the parameters (see Table S1 in the Supplemental Materials). In order to detect the flow transition from low flow to pressure flow, two different criteria are available in HEC-RAS: the energy grade line at the upstream cross section (default option) and the water surface elevation. Whereas the energy grade line is more conservative, the second option was selected in the numerical simulation.

In the energy method the curves are computed using the standard step method between two sets of consecutive cross sections placed upstream and downstream of the bridge: the two cross sections adjacent to the bridge can be modified to take into account the presence of ineffective flow areas, and two additional cross sections are taken inside of the bridge structure. The pressure-and-weir method for high-flow conditions combines different equations to model pressure flow (both in free and submerged condition), weir flow, and their possible combination.

The obtained rating curves for bridges are then used in 2D modeling to compute the difference between upstream and downstream water surface elevation. This difference is then used to compute a force that is distributed to the cells along the bridge centerline, where a special version of the momentum equation is solved. The amount of force given to each cell is based on the percentage of the total flow passing through that particular set of cells.

Numerical Tests

Steady-State Tests

A Cartesian mesh was built in the numerical simulations, testing the sensitivity of different mesh sizes on the water depth measured

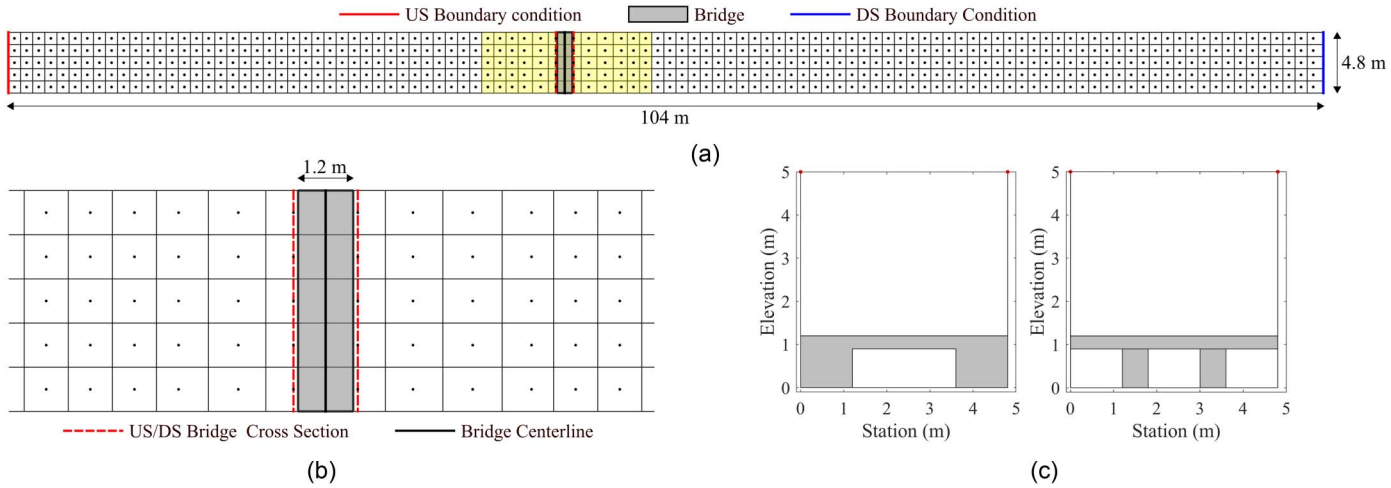

Fig. 1. Mesh and bridge layout used for the orthogonal set of bridges. (a) Numerical mesh adopted for the simulation, highlighting the location of the bridge and the upstream/downstream boundary condition; (b) details of the mesh around the bridge with the location of the upstream and downstream bridge cross sections used for the computation of the 1D rating curves; and (c) example of two bridge layouts used in the simulation (RECT1 and T1).

upstream of the bridge. The flume walls were defined as solid walls. Eventually, a mesh with an average linear size of around 0.96 m (0.048 m at the physical model scale) was used, except in correspondence of the bridge where the mesh was adapted to satisfy the requirements for bridge modeling. Provided that the flow is subcritical in the upstream stretch of the flume, the measured constant discharge was used as the upstream boundary condition until convergence to the steady-state solution; the depth measured at the end of the channel was used as the downstream boundary condition. The mesh and some of the bridges layout used for the orthogonal bridge set are shown in Fig. 1.

In some cases, the geometry and the location of the bridges required a mesh refinement and the introduction of an unstructured grid (Fig. S5 in the Supplemental Materials); in particular, for the RECT1 VERTICAL and RECT1 HORIZONTAL cases (see Fig. S3 in the Supplemental Materials), two fine digital elevation models were built to reproduce the geometry of the vertical and the horizontal abutments; consequently, the mesh cells were aligned to the geometry of the abutments, also respecting the constraints imposed by the other bridge modeling criteria in HEC-RAS. Furthermore, in the cases RECT1 OBLIQUE, ARC1 OBLIQUE, and T1 OBLIQUE (see Fig. S3 in the Supplemental Materials) the centerline of the bridge is oblique to the walls of the flume, and a mesh alignment was required. A selection of the computed water depths upstream of some bridges is shown in Fig. 2, where the symbols in the caption refer to those adopted by Ratia et al. (2014). The results for the remaining tested bridges are shown in Fig. S6 in the Supplemental Materials. The different shadings in Fig. 2 represent the three possible ranges of occurrence of low-flow, pressure, and overtopping conditions at each bridge. The shadings are intensified in the areas where the same hydraulic behavior occurs both in the experiments and in the numerical simulations. For the geometries with abutments (RECT1, RECT2, and ARC2; see also Fig. S3 in the Supplemental Materials), the possibility offered by HEC-RAS to introduce ineffective flow areas near the abutments was tested. In this case, a systematic underestimation of the level upstream especially for low-flow conditions was observed. An improvement was observed by eliminating the ineffective flow areas as shown in the following, where also the effect of the contraction (Cc) and expansion (Ce) energy loss coefficients is presented.

To quantify the matching between the observed data and the numerical results obtained using HEC-RAS 2D for each bridge, the mean absolute percentage error (MAPE) is computed and shown in Fig. 2. The MAPE is defined as follows:

$$\text{MAPE} = 100 \cdot \frac{1}{N} \sum_{i=1}^{N} \frac{|h_i^{\text{HR}} - h_i^{\text{EXP}}|}{h_i^{\text{EXP}}} \tag{2}$$

where N = total number of experimental points for each bridge geometry; h_i^{HR} = upstream water depth computed using HEC-RAS 2D; and h_i^{EXP} = upstream water depth measured during the steady experiments for each bridge. In the free-surface range, the results of the two methods are identical, and the triangles are not shown.

Dam Break Tests

Stoker-like dam breaks were simulated using a Cartesian mesh for the reservoir and the channel (Fig. 3), testing different mesh sizes (Fig. S7). Eventually, an average linear size of around 0.40 m (0.02 m at the physical model scale) was selected, except in correspondence of the bridge where the mesh was adapted to satisfy the requirements for bridge modeling; a different water level in the reservoir and in the flume was imposed as the initial condition. The flume walls were defined as solid walls. The results for three cases are shown in Fig. 4. Similar results are obtained for the other bridges tested, shown in the Supplemental Materials in Fig. S8.

Discussion

The obtained results in steady state show that the backwater profiles are very well-matched for almost all tested cases. Using the default set of coefficients, when the bridge is orthogonal to the main flow and the abutments are vertical, the match between computed and measured water depth upstream is excellent for low-flow conditions. For pressure conditions and overtopping conditions, the comparison slightly deteriorates. Table 1 shows the average error for the three flow conditions. Bridges orthogonal to the flow, oblique, and with sloping abutments are considered separately in the table for the energy method and for the pressure-and-weir method.

In general, one can observe a better performance of the energy method in steady test cases with respect to the pressure-and-weir method. The mean MAPE obtained pooling all the cases is 4.60%

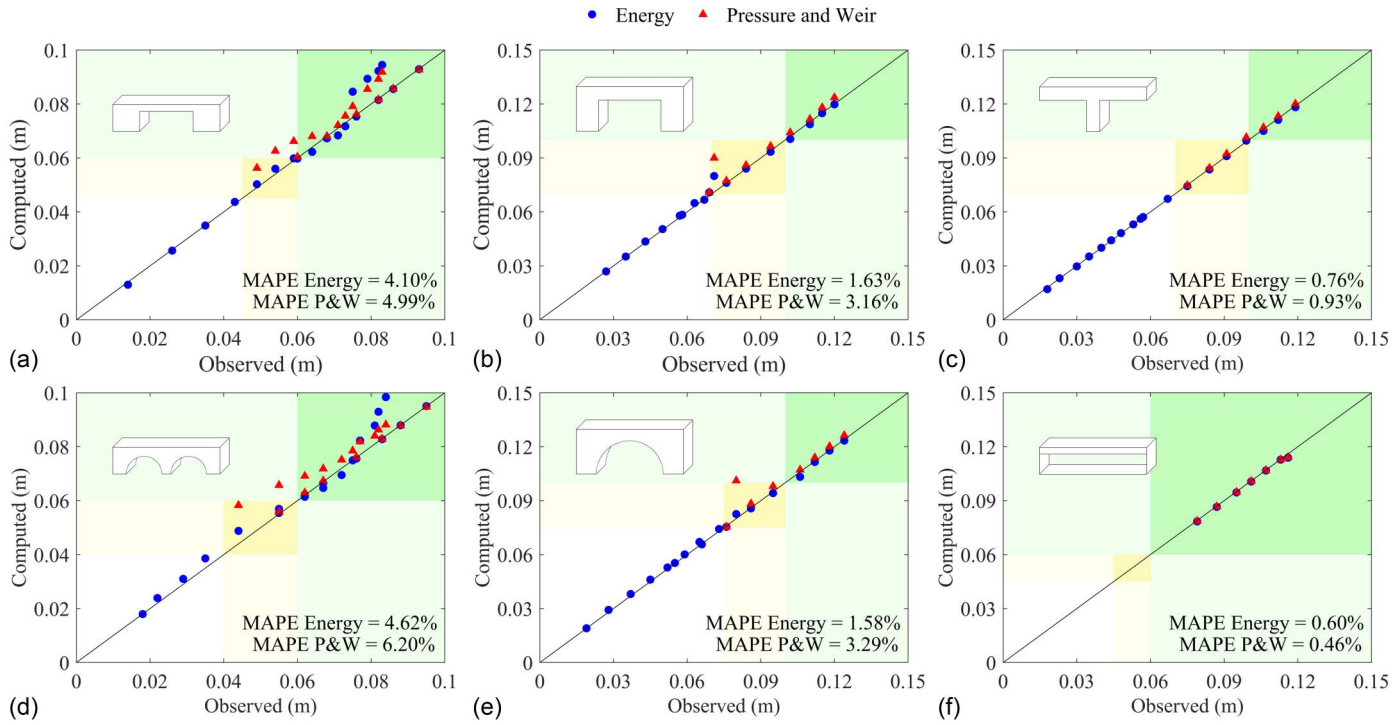

Fig. 2. Comparison between the observed data from the experiments and the results obtained with the energy and pressure-and-weir methods, using the set of default parameters. See the text for the meaning of the shadings: (a) RECT1; (b) RECT2; (c) T2; (d) ARC1; (e) ARC2; and (f) DECK2.

for the Energy method and 4.91% for the pressure-and-weir. On average, in the worst case, one can expect a maximum error of the upstream water elevation below 10%, which is very good for practical field applications.

Some of the bridges in Fig. 2 exert a flow contraction caused by their geometry. Accordingly, different expansion and contraction coefficients for energy loss were tested. As reported in the hydraulic reference manual (Brunner 2020) for 1D bridge modeling, the possible range of variation of the contraction and expansion loss coefficient is between 0 and 1 as an upper value for abrupt transition. Fig. 5 shows the variation range of the results obtained for the bridges in Figs. 2(a, b, and e), by varying the contraction and expansion loss coefficients within the suggested upper and lower bounds. Although the variation of the coefficients can improve the performance, it seems difficult to find out how and when to depart from the default values. Accordingly, also considering the limited error, it seems that using the default value of the parameters can be *a priori* suggested for all cases.

On the other hand, the combination of the ineffective flow areas (which leads to an underestimation of the upstream water surface for the bridge geometry RECT1, RECT2, and ARC2 when the default values for *Cc* and *Ce* are used) and the contraction and

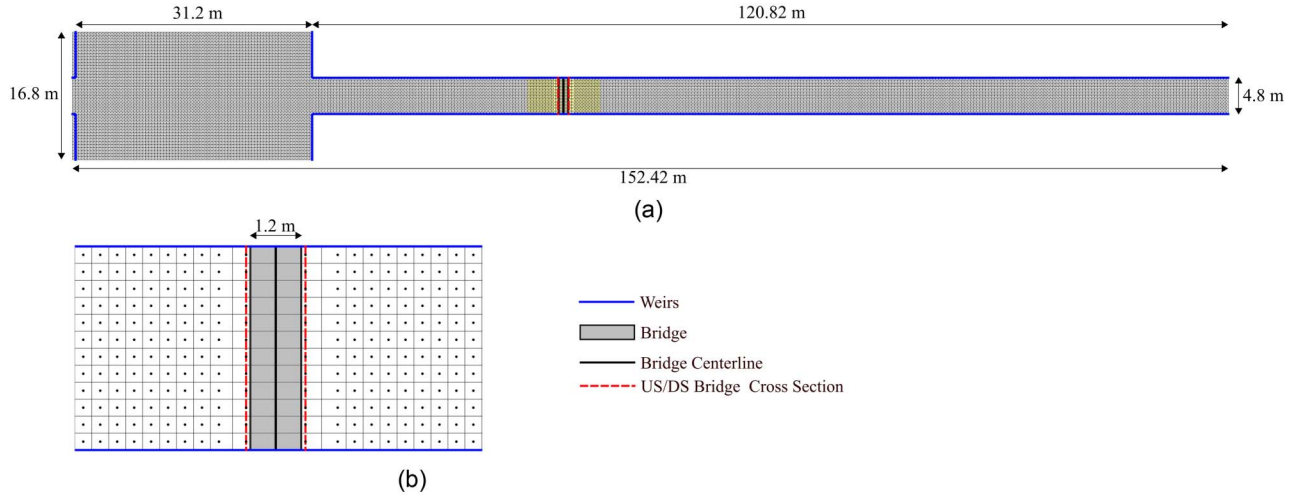

Fig. 3. Example of mesh and bridge layout used for the dam break test for RECT1 case: (a) numerical mesh adopted for the simulation, highlighting the location of the bridge; and (b) details of the mesh around the bridge with the location of the upstream and downstream bridge cross sections used for the computation of the 1D rating curves. Similar layouts characterize the other test cases.

J. Hydraul. Eng., 2026, 152(1): 06025013

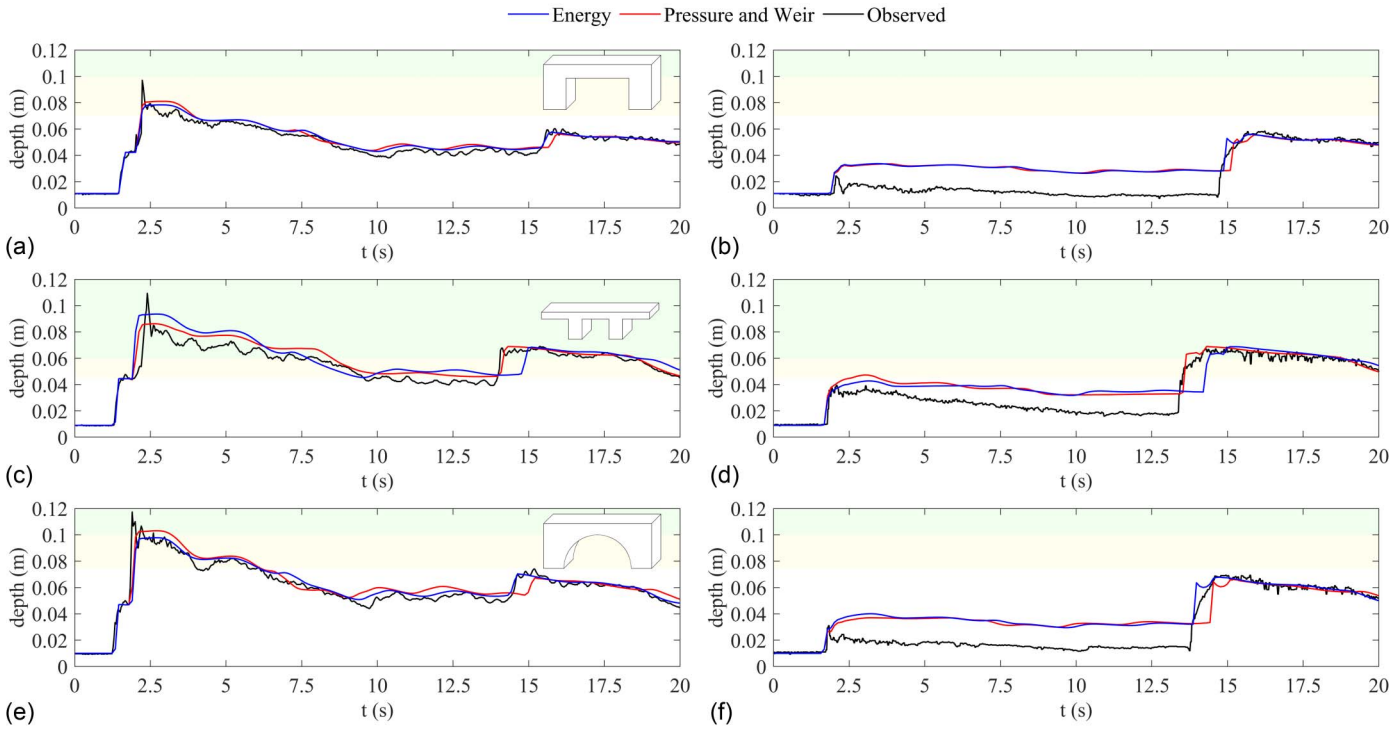

Fig. 4. Comparison of the results for dam break experiments obtained with HEC-RAS 2D, using energy and pressure-and-weir methods for bridge modeling. The results show the water depth upstream and downstream of the bridge: (a) TEST1 RECT2 US; (b) TEST1 RECT2 DS; (c) TEST1 T1 US; (d) TEST1 T1 DS; (e) TEST1 ARC2 US; and (f) TEST1 ARC2 DS.

Table 1. Mean absolute percentage error for the different categories of bridge under different flow conditions in steady flow: (1) energy method; and (2) pressure-and-weir method

Bridge type	Orthogonal		Oblique		Sloping abutments	
Flow condition	MAPE (1) (%)	MAPE (2) (%)	MAPE (1) (%)	MAPE (2) (%)	MAPE (1) (%)	MAPE (2) (%)
Low flow	1.9	1.9	12.6	12.6	9.4	9.4
Pressure flow	2.8	11.4	6.9	8.5	9.3	9.3
Overtopping	3.7	2.6	8.4	2.0	10.8	5.8

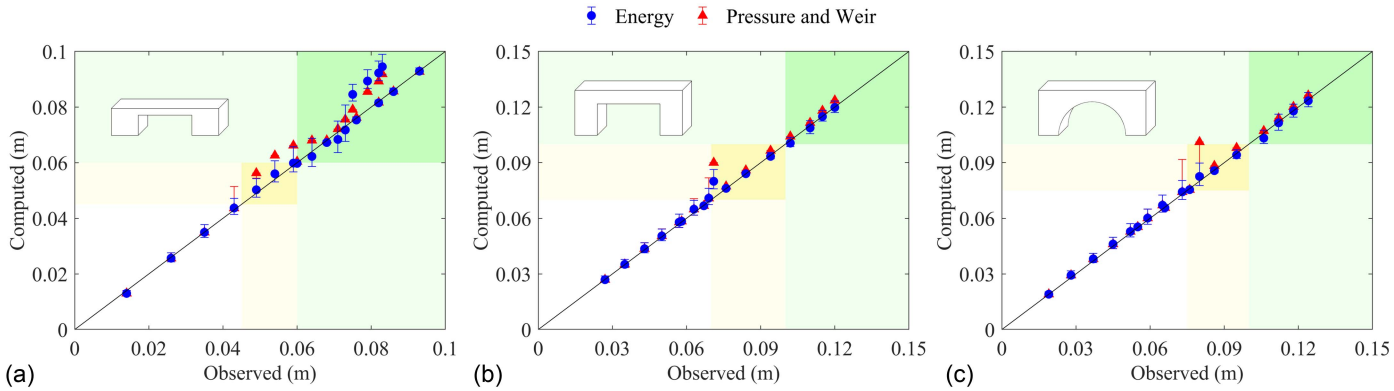

Fig. 5. Sensitivity of the bridge headwater with different contraction ($0.1 \leq Cc \leq 0.6$) and expansion ($0.3 \leq Ce \leq 0.8$) loss coefficient for cases: (a) RECT1; (b) RECT2; and (c) ARC2 in Fig. 2.

expansion loss coefficients that required calibration was investigated. The ineffective flow areas were located upstream and downstream covering the area occupied by the abutments up to the high chord of the bridge deck. Acting on the values of Cc and Ce a good match with the observed values could be achieved, as shown in Fig. 6.

Considering pressure flow in Figs. 2(a and b) (RECT1 and RECT2), the pressure-and-weir formulation slightly overestimates

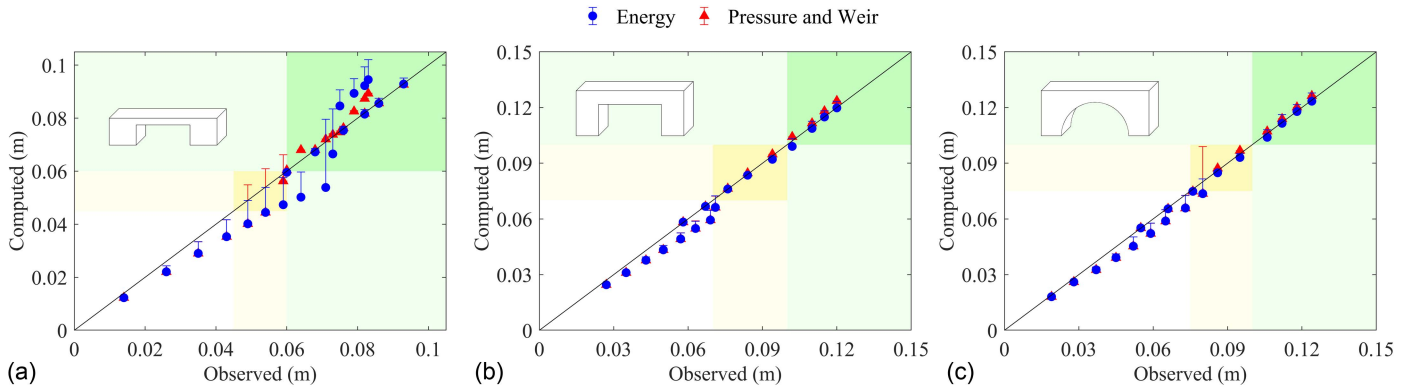

Fig. 6. Sensitivity of the bridge headwater using ineffective flow areas for the cases: (a) RECT1; (b) RECT2; and (c) ARC2 in Fig. 2. The solid dots and triangles represent the results obtained using the ineffective flow areas and the default values for Cc and Ce, whereas the ticks represent the improvements obtained acting on Cc and Ce to match the observation. (RECT1 $Cc = 0.8$ and $Ce = 1$, RECT2 $Cc = 0.6$ and $Ce = 0.8$, and ARC2 $Cc = 0.6$ and $Ce = 0.8$.)

the upstream water level, but on the other hand, the upstream water level is well captured in Fig. 2(c) (T2). Accordingly, the effects of the discharge coefficients for submerged inlet (C_d) and for submerged inlet and outlet (C) adopted in the pressure-and-weir method have been explored. In the default procedure C_d is computed as function of the degree of submergence upstream, according to a monotonically growing curve where the min and max values for C_d are, respectively, 0.27 and 0.5. On the other hand, if a value is defined by the user, C_d remains equal to the user's value for any degree of submergence upstream. Considering that the depth is overestimated, a sensitivity for the maximum value of C_d has been performed. The obtained results show that in the RECT1 and RECT2 cases there is limited improvement if $C_d = 0.5$ is used, without worsening the results for case T2.

Finally, the results in unsteady flow confirm the very good reproduction of the water depth upstream of the bridge. However, as one could expect from the hydrostatic nature of SWE, the impulsive elevation peak is almost always underrated, with a maximum error in the order of 20%. Furthermore, the simulations show that the solver does not reproduce the supercritical behavior immediately downstream of the bridge, where the water elevation is overrated until the arrival of the wave reflected from the downstream end of the channel. Note that in the steady-state experiments, the elevation downstream of the bridge is measured only at the end of the flume, far from the area affected by the bridge contraction. Accordingly, the same problem could also be present in steady state.

Whereas the correct reproduction of the behavior upstream of the bridge is fundamental for the flood extension, the flow field immediately downstream of the bridge contraction is important when local erosion is a concern. Therefore, it seems that further model validations are required for the application of the HEC-RAS model to predict scour around and downstream of bridge piers.

Conclusions

It is difficult to overstate the practical importance of bridge modeling in the overall framework of flood modeling, considering the role played by bridges on floodplain inundation. Moreover, it is well known that bridge modeling represents a complex area, largely due to their great geometric variability, which spans from a simple deck crossing a channel to irregular multiarch structures that interact with the flow for any stage. Accordingly, we believe that the validation of these components should begin with simplified and controlled conditions such as those provided by laboratory experience in a flume. In real situations the surrounding bathymetry could exert an additional level of complexity when the flow becomes strongly 3D; in any case it is of paramount importance that the geometric description of the bridge is well connected with the surrounding topography. The presented comparison of experimental data with computed results ranged between steady-state and dam break flows. The main conclusions are as follows:

- Under the assumption that the domain is correctly gridded in correspondence of the bridge, the elevation upstream of the tested bridges is very well reproduced when the bridge is orthogonal to the flow direction, both in steady and unsteady state. The quality of the solution slightly deteriorates when the axis of the bridge is oblique to the channel direction or in the presence of sloping abutments. Here it is important to underline that these bridge layouts introduce a certain degree of subjectivity in all the modeling setup and that the methodology to deal with skewed bridges is still in evolution in HEC-RAS versions.
- In general in steady test cases, the energy method seems to perform better than the pressure-and-weir method. The use of the default set of coefficients and of the standard value of the contraction and expansion coefficient provides a maximum error that, in the different flow conditions and for the different bridge layouts, is documented in Table 1. A back-of-the-envelope conservative evaluation of the maximum error is below 15%.
- The tests in unsteady flow, where the elevation is measured also downstream and close to the bridge, confirm the very good performance upstream of the bridge and show that the downstream supercritical stretch is not always correctly captured.

Data Availability Statement

Some or all data, models, or code generated or used during the study are available in a repository online in accordance with funder data retention policies: Ratia, H., Murillo, J., & García-Navarro, P. (2024). Data from: Numerical modelling of bridges in 2D shallow water flow simulations [Data set]. In International Journal for Numerical Methods in Fluids (Vol. 75, N. 4, pp. 250–272). https://doi.org/10.5281/zenodo.14230033.

Author Contributions

Gabriele Farina: Conceptualization; Investigation; Methodology; Software; Writing – original draft; Writing – review and editing. Marco Pilotti: Conceptualization; Methodology; Supervision; Writing – original draft; Writing – review and editing. Riccardo Bonomelli: Writing – original draft; Writing – review and editing. Sergio Martínez-Aranda: Data curation; Writing – original draft; Writing – review and editing. Pilar García-Navarro: Data curation; Writing – original draft; Writing – review and editing.

Notation

The following symbols are used in this paper:

C = discharge coefficient for submerged inlet and outlet;
Cc = contraction loss coefficient;
Ce = expansion loss coefficient;
C_d = discharge coefficient for submerged inlet;
g = gravity acceleration;
$h^{\exp}$ = upstream water depth measured in steady-state experiments;
h^{HR} = upstream water depth computed with HEC-RAS 2D;
L_m = model characteristic length;
L_p = physical model characteristic length;
MAPE = mean absolute percentage error;
N = total number of experimental points;
n_m = model Manning coefficient;
n_p = physical model Manning coefficient;
Q_m = model volumetric discharge;
Q_p = physical model volumetric discharge;
R = Reynolds number;
t_m = model time;
t_p = physical model time;
v_m = model velocity;
v_p = physical model velocity;
λ_l = length scale;
λ_t = time scale;
λ_v = scale ratio for velocity;
λ_Q = scale ratio for volumetric discharge; and
λ_n = scale ratio for Manning coefficient.

Supplemental Materials

Text S1, Figs. S1–S8, and Table S1 are available online in the ASCE Library (www.ascelibrary.org).

References

Bradley, J. N. 1978. *Hydraulics of bridge waterways*. Washington, DC: US Department of Transportation Federal Highway Administration.

Brunner, G. W. 2020. *HEC-RAS, river analysis system hydraulic reference manual*. Davis, CA: USACE.

Brunner, G. W., A. Sanchez, T. Molls, and D. A. Parr. 2020. *HEC-RAS verification and validation tests*. Davis, CA: USACE.

Caviedes-Voullième, D., M. Morales-Hernández, M. R. Norman, and I. Özgen-Xian. 2023. "SERGHEI (SERGHEI-SWE) v1.0: A performance-portable high-performance parallel-computing shallow-water solver for hydrology and environmental hydraulics." *Geosci. Model Dev.* 16 (3): 977–1008. https://doi.org/10.5194/gmd-16-977-2023.

Cea, L., and A. López-Núñez. 2021. "Extension of the two-component pressure approach for modeling mixed free-surface-pressurized flows with the two-dimensional shallow water equations." *Int. J. Numer. Methods Fluids* 93 (3): 628–652. https://doi.org/10.1002/fld.4902.

Cea, L., G. Vila, G. García-Alén, J. Puertas, and L. Pena. 2022. "Hydraulic modeling of bridges in two-dimensional shallow water models." *J. Hydraul. Eng.* 148 (8): 06022006. https://doi.org/10.1061/(asce)hy.1943-7900.0001992.

Chanson, H. 2004. *The hydraulics of open channel flows: An introduction*. 2nd ed. Oxford, UK: Elsevier.

Chu, C.-R., C.-H. Chung, T.-R. Wu, and C.-Y. Wang. 2016. "Numerical analysis of free surface flow over a submerged rectangular bridge deck." *J. Hydraul. Eng.* 142 (12): 04016060. https://doi.org/10.1061/(ASCE)HY.1943-7900.0001177.

Costabile, P., C. Costanzo, D. Ferraro, and P. Barca. 2021. "Is HEC-RAS 2D accurate enough for storm-event hazard assessment? Lessons learnt from a benchmarking study based on rain-on-grid modelling." *J. Hydrol.* 603 (Dec): 126962. https://doi.org/10.1016/j.jhydrol.2021.126962.

Costabile, P., C. Costanzo, J. Kalogiros, and V. Bellos. 2023. "Toward street-level nowcasting of flash floods impacts based on HPC hydrodynamic modeling at the watershed scale and high-resolution weather radar data." *Water Resour. Res.* 59 (10): e2023WR034599. https://doi.org/10.1029/2023wr034599.

Darji, K., D. Patel, I. Prakash, and H. A. Altuwaijri. 2024. "Hydrodynamic modeling of dam breach floods for predicting downstream inundation scenarios using integrated approach of satellite data, unmanned aerial vehicles (UAVs), and Google Earth Engine (GEE)." *Appl. Water Sci.* 14 (9): 187. https://doi.org/10.1007/s13201-024-02253-9.

Dazzi, S., R. Vacondio, and P. Mignosa. 2020. "Internal boundary conditions for a GPU-accelerated 2D shallow water model: Implementation and applications." *Adv. Water Resour.* 137 (Mar): 103525. https://doi.org/10.1016/j.advwatres.2020.103525.

Lai, Y. G., X. Liu, F. A. Bombardelli, and Y. Song. 2022. "Three-dimensional numerical modeling of local scour: A state-of-the-art review and perspective." *J. Hydraul. Eng.* 148 (11): 03122002. https://doi.org/10.1061/(ASCE)HY.1943-7900.0002019.

Maranzoni, A., and P. Mignosa. 2018. "Numerical treatment of a discontinuous top surface in 2D shallow water mixed flow modeling." *Int. J. Numer. Methods Fluids* 86 (4): 290–311. https://doi.org/10.1002/fld.4418.

Mckenna, J., V. Glenis, and C. Kilsby. 2023. "A new riemann solver for modelling bridges in flood flows—Development and experimental validation." *Appl. Math. Comput.* 447 (Jun): 127870. https://doi.org/10.1016/j.amc.2023.127870.

Milanesi, L., and M. Pilotti. 2021. "Coupling flood propagation modeling and building collapse in flash flood studies." *J. Hydraul. Eng.* 147 (12): 04021047. https://doi.org/10.1061/(asce)hy.1943-7900.0001941.

Mudashiru, R. B., N. Sabtu, I. Abustan, and W. Balogun. 2021. "Flood hazard mapping methods: A review." *J. Hydrol.* 603 (Dec): 126846. https://doi.org/10.1016/j.jhydrol.2021.126846.

Petaccia, G., and E. Persi. 2024. "Improving a 1D hydraulic model to include bridges as internal boundary conditions." *Water* 16 (17): 2555. https://doi.org/10.3390/w16172555.

Pilotti, M., L. Milanesi, V. Bacchi, M. Tomirotti, and A. Maranzoni. 2020. "Dam-break wave propagation in alpine valley with HEC-RAS 2D: Experimental Cancano test case." *J. Hydraul. Eng.* 146 (6): 05020003. https://doi.org/10.1061/(asce)hy.1943-7900.0001779.

Ratia, H., J. Murillo, and P. García-Navarro. 2014. "Numerical modelling of bridges in 2D shallow water flow simulations." *Int. J. Numer. Methods Fluids* 75 (4): 250–272. https://doi.org/10.1002/fld.3892.

Seckin, G., T. Haktanir, and D. W. Knight. 2007. "A simple method for estimating flood flow around bridges." *Proc. Inst. Civ. Eng. Water Manage.* 160 (4): 195–202. https://doi.org/10.1680/wama.2007.160.4.195.